Study of scattering from time-varying Gerstners sea surface using second-order small slope approximation*

Zhang Yan-Min(张彦敏)[a], Wang Yun-Hua(王运华)[b]†, and Guo Li-Xin(郭立新)[c]

[a] *Department of Physics, Ocean University of China, Qingdao* 266100, *China*
[b] *Ocean Remote Sensing Key Laboratory of Ministry of Education, Ocean University of China, Qingdao* 266003, *China*
[c] *School of Science, Xidian University, Xi'an* 710071, *China*

(Received 12 September 2009; revised manuscript received 20 October 2009)

Backscattered fields from one-dimensional time-varying Gerstners sea surface are calculated utilising the second-order small slope approximation. It is well known that spectral properties of the backscattered echoes relate to the velocity of the small elementary scatterers on sea surface profiles. Therefore, modeling Doppler spectra from the ocean requires an accurate description of the sea surface motion. The profile of nonlinear Gerstners sea surface shows vertical-skewness of sea waves, it is sharper at the crest and flatter at the trough than linear waves, and its maximum slope position is closer to the crest than to the trough. Furthermore, the horizontal component of the small elementary scatterers orbit velocity on the sea surface, which yields noticeable influence on Doppler spectra, can be obtained conveniently by Gerstners sea surface model. In this study, the characteristics of Doppler spectra of backscattered fields from time-varying Gerstners sea surface are investigated and the dependences of the Doppler frequency and the Doppler bandwidth on the parameters, such as the wind speed, the radar frequency, the incident angle, etc. are discussed. It is shown that the Doppler bandwidth of microwave scattered fields from Gerstners sea surface is considerably broadened. For the case of high frequency backscattered fields, the values of the higher-order spectrum peaks are larger than those obtained by linear sea surface.

Keywords: Gerstners sea surface, electromagnetic scattering, Doppler spectra, second-order small slope approximation

PACC: 4120, 4110H

1. Introduction

The study of electromagnetic scattering from time-evolving oceanic surface has been the subject of intensive investigation over the past several decades for its application in a number of important research areas such as oceanic remote sensing, target detecting or tracking embedded in the sea. It is well known that an adapted sea surface model is important for numerical simulations of radar backscattered signals.[1−6] Generally, linear sea surface model, which is a linear superposition of free waves with random phases, is employed to generate the oceanic surface profile.[1−5] However, it is now well established that the wave-wave interactions between harmonic waves cannot be neglected if one aims at interpreting the Doppler spectra of backscattered fields.[7−9] Furthermore, the horizontal components of the small surface elementary scatterers orbit velocity, which yields a noticeable influence on the Doppler spectrum, can not be obtained by the linear model directly. Gerstners sea surface model[10,11] is an exact solution of nonlinear hydrodynamic equations for surface gravity waves for water of infinite depth. In this model, the nonlinear interactions in the surface evolution have been considered and the geometrical structure of Gerstners waves is similar to the structure of Stokes waves in many important respects, such as the vertical-skewness of sea waves. Moreover, Gerstners waves model is rotational, and then the horizontal component of the small elementary scatterers orbit velocity on Gerstners sea surface can be obtained conveniently. As mentioned above, this horizontal component of orbit velocity also impacts on the behaviours of the Doppler spectra. So it is significant to explore the characteristics of electromagnetic scattering from Gerstners sea surface.

In this work, a numerical electromagnetic method based on the second-order small slope approximation

*Project supported by the Young Scientists Fund of the National Natural Science Foundation of China (Grant No. 40906088), the National Natural Science Foundation of China (Grant No. 60971067) and Specialised Research Fund for the Doctoral Program of Higher Education (Grant No. 200804231021).

†Corresponding author. E-mail: wyh78917@ouc.edu.cn

© 2010 Chinese Physical Society and IOP Publishing Ltd

(SSA-II)[12] is utilised to evaluate the backscattered returns of one-dimensional 1-D Gerstners sea surface for various radar frequencies, wind speeds and incident angles. It should be pointed out that the prediction of the sea surface average Doppler spectra requires a Monte Carlo simulation in which scattering calculations are performed at a series of time steps as surface realisations evolve. Although scattering from two-dimensional (2-D) surfaces have also been reported in many reports, the requirement of repeated calculations for multiple realisations at multiple time steps prevents Doppler studies with 2-D time-varying sea surface at present.

This paper is organised as follows. In Section 2, the outlines of the Gerstners sea surface model are described. At the same time, the comparisons between Gerstners and Stokes wave are also presented. Then we present the properties of orbit velocity of small surface elementary on Gerstners sea surface. Section 3 presents the electromagnetic (EM) model for Gerstners sea surface while Section 4 is devoted to the results and the comments. The paper ends with Section 5 for concluding remarks and perspectives.

2. Gerstners sea surface model

The time-varying Gerstners sea surface model can be described as follows[10]

$$\begin{aligned} & z(x,t) \\ = & \int \{F(K)\exp[\mathrm{j}(Kx_0-\omega t+\Phi_n)]+\text{c.c.}\}\,\mathrm{d}K, \\ & x(x_0,t) \\ = & x_0+\int \{\mathrm{j}F(K)\exp[\mathrm{j}(Kx_0-\omega t+\Phi_n)]+\text{c.c.}\}\,\mathrm{d}K, \end{aligned} \tag{1}$$

where, $\mathrm{j}=\sqrt{-1}$, K and Φ_n denote the spatial wave number and the random phase of harmonic wave, respectively. $\omega=\sqrt{gK+(K/K_\mathrm{m})^2}$, g is the gravity acceleration constant. And K_m is related to the surface tension η and the water density ρ as $K_\mathrm{m}=\sqrt{\rho g/\eta}$, c.c. denotes complex conjugate. In Eq. (1), $F(K)=\sqrt{LW(K)/4\pi}$, L denotes the width of the surface, and the Pierson–Moskowitz sea surface spectrum $W(K)$ can be written as[1]

$$W(K)=\frac{\alpha}{4|K|^3}\exp\left(-\frac{\beta g^2}{K^2U_{19.5}^4}\right), \tag{2}$$

where $\alpha=8.10\times10^{-3}$, $\beta=0.74$, and $U_{19.5}$ is the wind speed at a height of 19.5 m over the sea surface. In Eq. (1), the linear sea surface model is obtained by setting $x=x_0$.

Taking the time derivative of Eq. (1), the orbit velocities of small elementary scatterers on the sea surface are given by

$$\begin{aligned} & V_z(x,t) \\ = & \int \{-\mathrm{j}\omega F(K)\exp[\mathrm{j}(Kx_0-\omega t+\Phi_n)]+\text{c.c.}\}\,\mathrm{d}K, \\ & V_x(x,t) \\ = & \int \{\omega F(K)\exp[\mathrm{j}(Kx_0-\omega t+\Phi_n)]+\text{c.c.}\}\,\mathrm{d}K, \end{aligned} \tag{3}$$

where, V_z and V_x represent the vertical and horizontal components of orbit velocity, respectively.

In order to display the properties of the Gerstners sea surface clearly, in the following, only a single harmonic wave is considered and then it is obtained as

$$\begin{aligned} z(x,t) &= A\cos[Kx_0-\omega t+\Phi], \\ x(x_0,t) &= x_0-A\sin[Kx_0-\omega t+\Phi]. \end{aligned} \tag{4}$$

Employing the successive approximation method, Eq. (4) can be rewritten as

$$\begin{aligned} z(x,t) \approx & \frac{1}{2}KA^2+A\cos(Kx-\omega t+\Phi) \\ & +\frac{1}{2}KA^2\cos[2\cdot(Kx-\omega t+\Phi)] \\ & +\frac{3}{8}K^2A^3\cos[3\cdot(Kx-\omega t+\Phi)] \\ & -\frac{3}{8}K^2A^3\cos(Kx-\omega t+\Phi)\ldots. \end{aligned} \tag{5}$$

As it is well known that the Stokes wave up to third order in deep water is given by[13]

$$\begin{aligned} z(x,t) = & \frac{1}{2}KA^2+A\cos(Kx-\omega t+\Phi) \\ & +\frac{1}{2}KA^2\cos[2\cdot(Kx-\omega t+\Phi)] \\ & +\frac{3}{8}K^2A^3\cos[3\cdot(Kx-\omega t+\Phi)]\ldots. \end{aligned} \tag{6}$$

By comparison, it is obvious that Eq. (5) coincides with Eq. (6) exclusive of the last term. The first-order term, i.e. the second term in Eq. (5), corresponds to linear wave. The third and the forth terms, which are caused by wave-wave interactions, are nonlinear terms.

Figures 1(a) and 1(b) show the comparisons between Gerstners and the linear sea surface model. Here, the wind speed is 6 m/s. From Fig. 1, it is found that the profile shape of Gerstners sea surface shows vertical-skewness of sea waves, it is sharper at the crest and flatter at the trough than linear wave, and its maximum slope position is closer to the crest than to the trough. These characteristics of Gerstners sea surface are more consistent with the actual sea waves.[13]

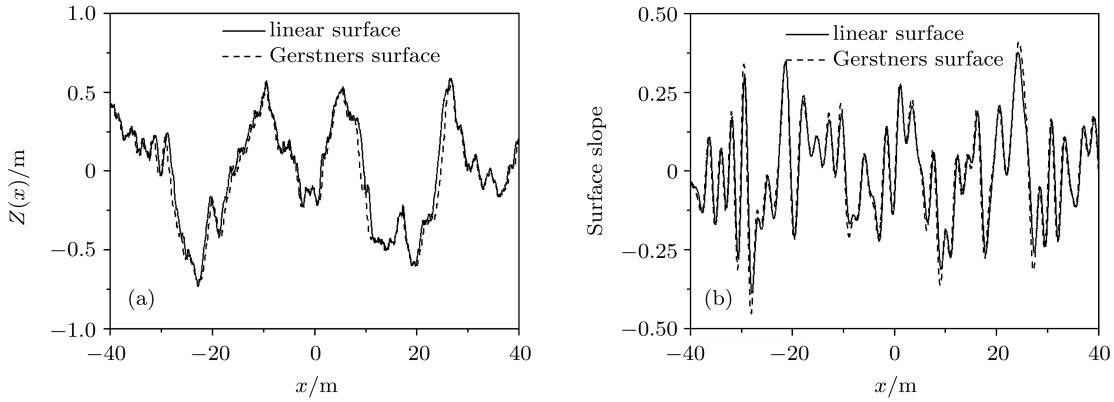


Fig. 1. Comparison of sea surface profiles corresponding to Gerstners and the linear model. (a) Sea surface profiles, (b) slope of sea surface profiles.

In Fig. 2, the properties of the orbit velocity on Gerstners sea surface are illustrated. Here, the wind speed is the same as in Fig. 1. As shown in Fig. 2, the magnitude of the horizontal component of orbit velocity is roughly equal to the magnitude of the vertical component. Therefore, this horizontal component must be considered in the process of simulating the Doppler spectra of scattered echoes.

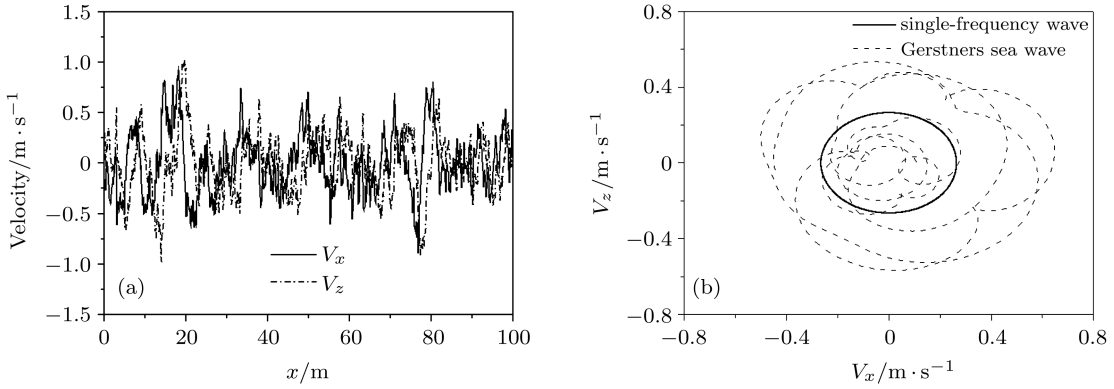


Fig. 2. The orbit velocity of small surface element on Gerstners sea surface. (a) Velocity versus abscissas, (b) orbit velocity of a special surface element.

3. SSA-II model of EM scattering by Gerstners sea surface

Suppose a tapered plane wave is incident on the sea surface and is given by[14]

$$E^{\rm in} = T(x, z, \theta_{\rm i}) \cdot \exp[{\rm j}k(x\sin\theta_{\rm i} - z\cos\theta_{\rm i})], \tag{7}$$

where, k denotes the wavenumber of incident wave, the incident angle $\theta_{\rm i}$ is defined with respect to the z axis and is positive in the counterclockwise direction, and the taper function $T(x, z, \theta_{\rm i})$ can be written as

$$T(x, z, \theta_{\rm i}) = \exp\left\{-\frac{(x + z\tan\theta_{\rm i})^2}{W^2} - {\rm j}\frac{k(x\sin\theta_{\rm i} - z\cos\theta_{\rm i})}{(kW\cos\theta_{\rm i})^2} \times \left[\frac{2(x + z\tan\theta_{\rm i})^2}{W^2} - 1\right]\right\}. \tag{8}$$

In Eq. (8), W is the parameter that controls the beam waist.

For the case that an incident plane wave is considered, SSA-II expression for linear conductive surface can be found in Ref. [12]. By introducing the taper function $T(x, z, \theta_{\rm i})$, the scattering field $E_{\rm p}^{\rm s}$ predicted by SSA-II has the following form

$$\begin{aligned} E_{\rm p}^{\rm s}(r_0, t) = {} & \frac{\sqrt{k}\exp(-{\rm j}kr_0 + \pi/4)}{\sqrt{2\pi\, r_0}} D^{\rm pp} \int T(x, z, \theta_{\rm i}) \cdot \exp\{{\rm j}[v_z z(x, t) - v_x x]\}\,{\rm d}x \\ & \times \left(1 - \frac{-{\rm j}}{4B^{\rm pp}} \int [B_1^{\rm pp} + B_2^{\rm pp} + 2k(\cos\theta_{\rm i} + \cos\theta_{\rm s})B^{\rm pp}] Z(\xi)\exp({\rm j}\xi x)\,{\rm d}\xi\right), \end{aligned} \tag{9}$$

where the superscript pp represents HH (horizontal) or VV (vertical) polarisation HH-Pol or VV-Pol,

$$v_x = k(\sin\theta_\mathrm{s} - \sin\theta_\mathrm{i}), \tag{10}$$

$$v_z = k(\cos\theta_\mathrm{s} + \cos\theta_\mathrm{i}), \tag{11}$$

$$D^{\mathrm{HH}} = -2\frac{\cos\theta_\mathrm{s}\cos\theta_\mathrm{i}}{\cos\theta_\mathrm{s} + \cos\theta_\mathrm{i}}, \tag{12}$$

$$D^{\mathrm{VV}} = 2\frac{1 - \sin\theta_\mathrm{s}\sin\theta_\mathrm{i}}{\cos\theta_\mathrm{s} + \cos\theta_\mathrm{i}}, \tag{13}$$

and the parameters B, B_1 and B_2 can be found in Ref. [12].

$$Z(\xi) = \frac{1}{2\pi}\int z(x)\exp(-\mathrm{j}\xi x)\,\mathrm{d}x \tag{14}$$

is a Fourier transform of the sea surface profile $z(x)$.

Substituting Eq. (1) into Eq. (9), the expression of scattered fields from Gerstners sea surface is obtained as

$$E_p^s(r_0,t) = \frac{\sqrt{k}\exp(-\mathrm{j}kr_0 + \pi/4)}{\sqrt{2\pi\, r_0}} D^{\mathrm{pp}} \int T(x_0,z,\theta_\mathrm{i})\cdot\exp\{\mathrm{j}[v_z z(x_0,t) - v_x x(x_0,t)]\}[1-\Delta(x_0,t)]\,\mathrm{d}x_0$$
$$\times\left(1 - \frac{\mathrm{j}}{4B^{\mathrm{pp}}}\int [B_1^{\mathrm{pp}} + B_2^{\mathrm{pp}} + 2k(\cos\theta_\mathrm{i} + \cos\theta_\mathrm{s})B^{\mathrm{pp}}]Z(\xi)\times\exp[\mathrm{j}\xi x(x_0,t)]\,\mathrm{d}\xi\right). \tag{15}$$

Here, the relation between $\mathrm{d}x$ and $\mathrm{d}x_0$ has been utilised. $z(x_0,t)$ and $x(x_0,t)$ are defined by Eq. (1), and the parameter $\Delta(x_0,t)$ is expressed as

$$\Delta(x_0,t) = \int \{KF(K)\exp[\mathrm{j}(Kx_0 - \omega t + \Phi_n)] + \mathrm{c.c.}\}\,\mathrm{d}K. \tag{16}$$

The Doppler spectrum is a power spectral density of the random time-varying complex amplitude of the scattered field E_p^s [c.f. Eq. (15)]. To evaluate it, we used a standard spectral estimation technique, i.e. the periodogram method. Then the expression of the Doppler spectra is given by

$$S(f) = \left\langle \frac{1}{T}\left|\int_0^T E_p^s(r_0,t)\,\mathrm{e}^{-\mathrm{j}2\pi ft}\,\mathrm{d}t\right|^2\right\rangle, \tag{17}$$

where, $\langle\bullet\rangle$ denotes ensemble average.[1]

The Doppler frequency and the Doppler bandwidth are defined as[15,16]

$$f_\mathrm{c} = \frac{\int fS(f)\,\mathrm{d}f}{\int S(f)\,\mathrm{d}f}, \tag{18}$$

and

$$W_\mathrm{f} = \sqrt{\frac{\int (f-f_\mathrm{c})^2 S(f)\,\mathrm{d}f}{\int S(f)\,\mathrm{d}f}}. \tag{19}$$

4. Numerical results and discussions

It is instructive to compare the normalised radar cross section (NRCS) produced by MoM, which is an exact numerical simulation, and the model Eq. (15). In Figs. 3 and 4, the bi-static NRCSs for one realisation of Gerstners sea surface and different radar frequencies are shown. Here, the incident angle is 45°, the sea surface length is $L = 136.5\lambda$ and the beam waist $W = L/6$. From the figures, one can find that the normalised radar cross sections evaluated by Eq. (15) show good agreement with the results obtained by MoM at almost all scattering angles.

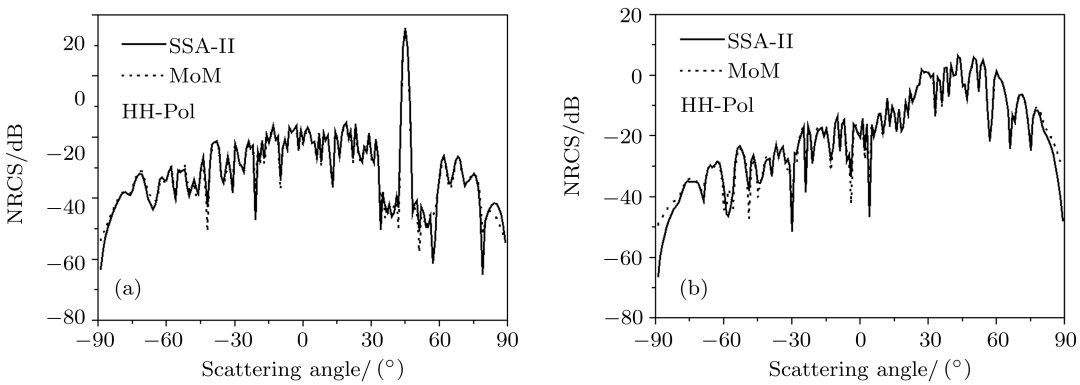


Fig. 3. NRCS by Gerstners sea surface at 5 m/s wind speed. (a) The radar frequency is 40 MHz, (b) the radar frequency is 1.3 GHz.

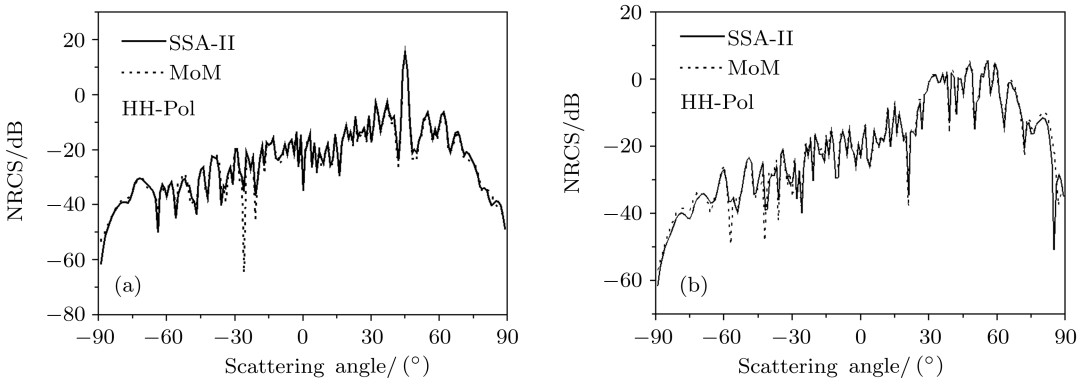


Fig. 4. NRCS by Gerstners sea surface at 8 m/s wind speed. (a) The radar frequency is 40 MHz, (b) the radar frequency is 1.3 GHz.

The mono-static average NRCSs for different wind speeds are shown in Figs. 5 and 6. Here, the cross sections were calculated by averaging the results over 80 realisations of sea surfaces. The sea surface length is $L = 136.5\lambda$ and the beam waist $W = L/6$. The radar frequencies in Figs. 5 and 6 are equal to 40 MHz and 1.3 GHz, respectively. From Figs. 5 and 6, it is shown that the NRCSs of Gerstners sea surfaces are somewhat larger than the scattered results from linear sea surfaces as the incident angle is large. This phenomenon can be explained by the reason that Gerstners sea surface includes wave–wave interactions. From Figs. 5 and 6, we can also find that the difference between the scattered results from the linear and Gerstners sea surfaces is getting larger with the increase of the radar frequency.

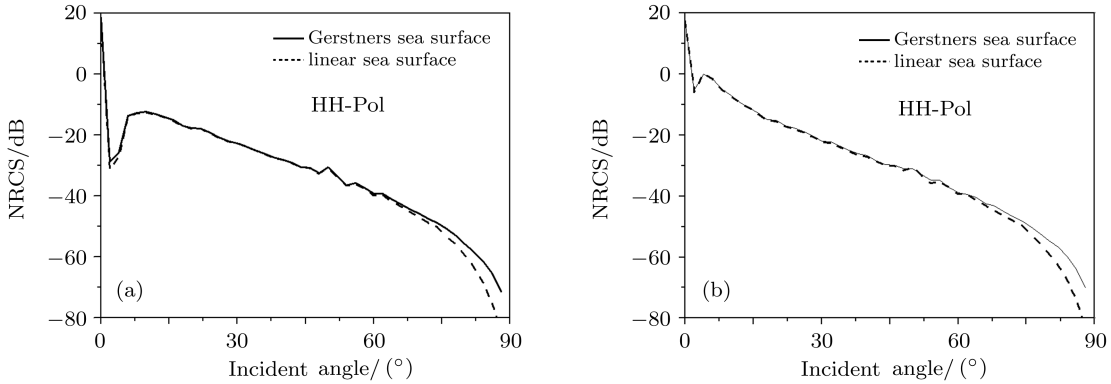


Fig. 5. Mono-static NRCS of high frequency wave versus incident angle for various wind speeds; radar frequency f_{r} is 40 MHz. (a) $U_{19.5} = 5$ m/s, (b) $U_{19.5} = 8$ m/s.

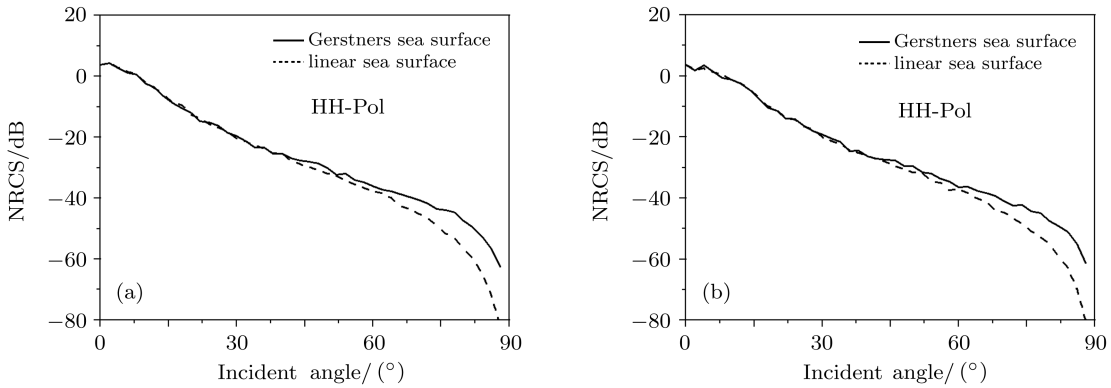


Fig. 6. Mono-static NRCS versus incident angle for various wind speeds; the radar frequency f_{r} is 1.3 GHz. (a) $U_{19.5} = 5$ m/s, (b) $U_{19.5} = 8$ m/s.

In the following, the Monte Carlo Doppler simulations using SSA-2 (c.f. Eq. (15)) were conducted at the radar frequencies $f_r = 40$ MHz and $f_r = 1.3$ GHz. The wind speed was chosen to be 5 m/s. The sea surface length $L = 136.5\lambda$, and the tapered incident field had a waist of $L/6$. Here, the Monte Carlo simulations used 10 realisations of linear or Gerstners surfaces. For the case of $f_r = 40$ MHz, sea surface evolved over a period of 102.4 s with a time step of 0.4 s. And for the case of $f_r = 1.3$ GHz, sea surface evolved over a period of 5.12 s with a time step of 0.02 s.

Figure 7 shows the comparisons of the Doppler spectra of the backscattered echoes from Gerstners and linear sea surface at the radar frequency $f_r = 40$ MHz. In Fig. 7, the vertical dash dot lines represent the Bragg frequencies.[17] As shown in Fig. 7, in all cases, the values of the first order Doppler peaks for linear sea surfaces are in agreement with the corresponding values for Gerstners sea surface. As mentioned above, the first order term in Gerstners model corresponds to linear waves (c.f. Eq. (5)). Based on the first order Bragg resonance theory,[18] the first order Doppler peaks for linear sea surfaces should be in agreement with the counterparts for Gerstners sea surface. However, the values of the higher order Doppler peaks for Gerstners sea surface are somewhat larger than those obtained by linear surface due to the nonlinear wave–wave interactions. All these conclusions are consistent with those obtained in Ref. [18].

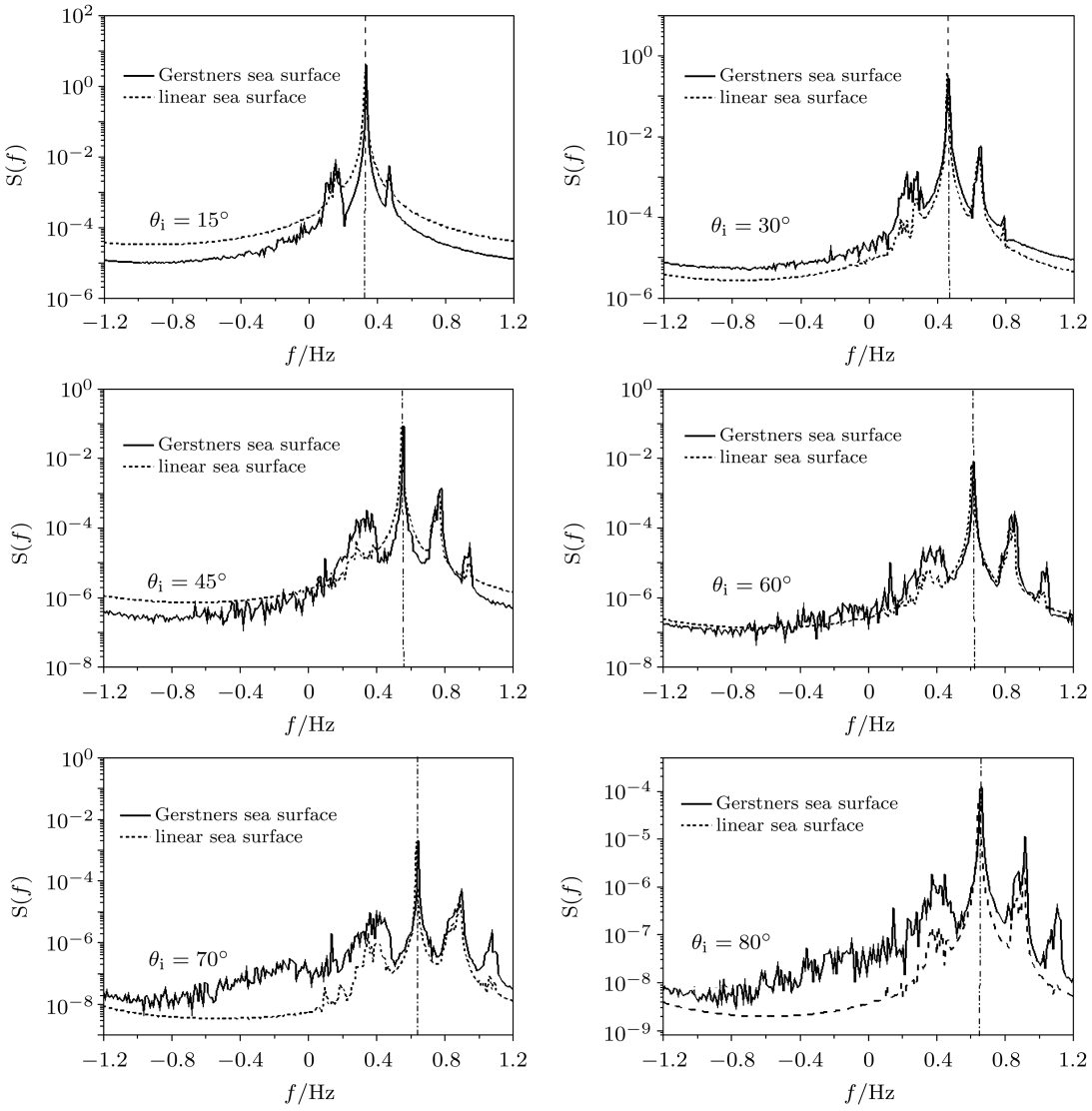


Fig. 7. Comparison of the average Doppler spectra corresponding to backscattering from Gerstners and linear sea surface for different incident angles at 5 m/s wind speed. $f_r = 40$ MHz.

The Doppler spectra of microwave scattered fields are presented in Fig. 8. Here, the radar frequency $f_r = 1.3$ GHz, and the wind speed is 5 m/s. In this figure, the vertical dash dot lines represent the Bragg frequencies. From Fig. 8, it is obvious that the spectra for Gerstners sea surfaces are considerably broader than their counterparts for the linear surfaces at the large incident angles due to the horizontal components of the small elementary scatterers orbit velocity and the wave–wave interactions in Gerstners sea surface model. This behaviour of the Doppler spectra is in qualitative agreement with experimental measurements, e.g., Ref. [19].

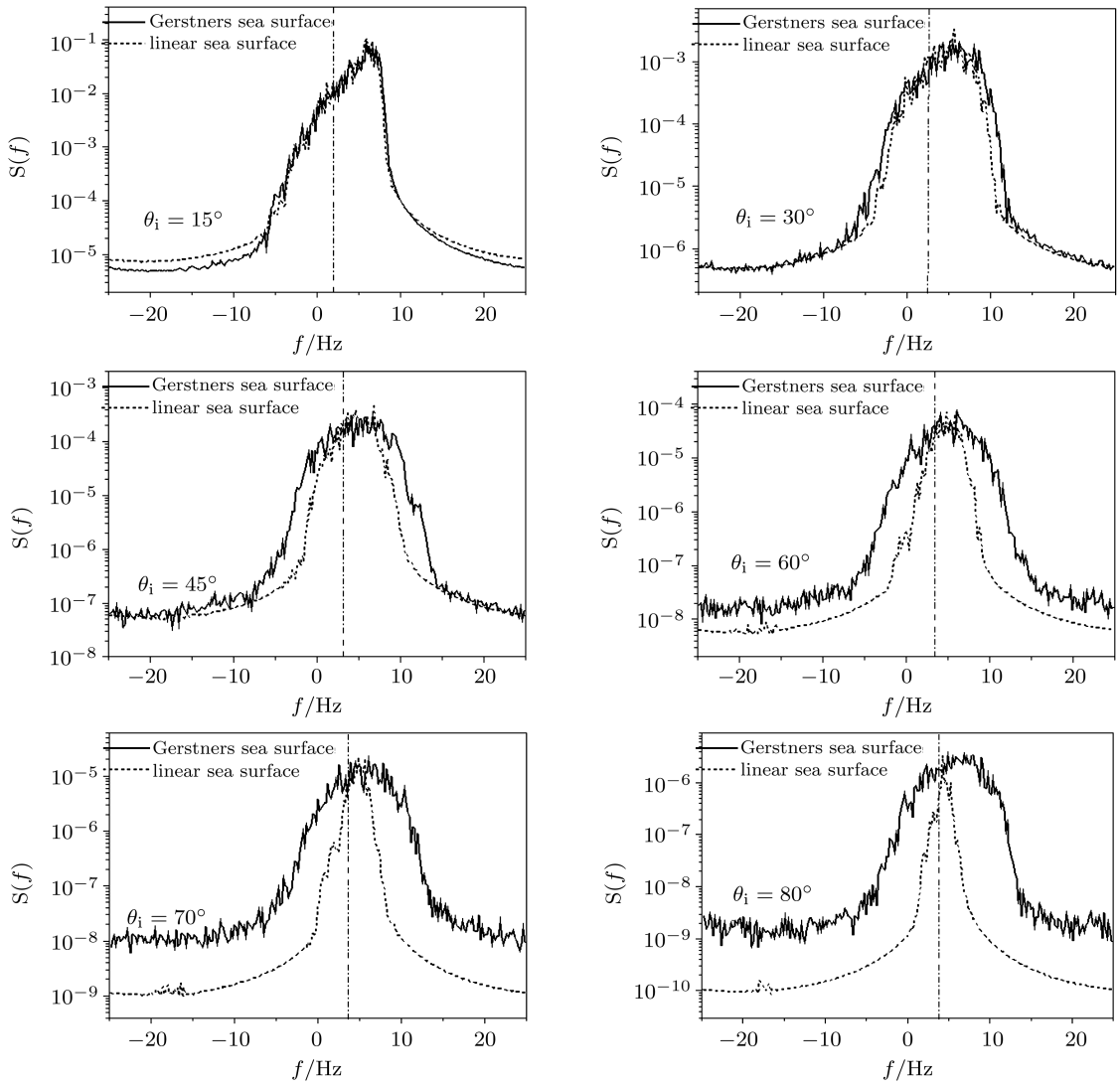


Fig. 8. Comparison of the average Doppler spectra corresponding to backscattering from Gerstners and linear sea surface for different incident angle.

In Figs. 3–8, only HH-Pol case has been considered due to the limited length of the article, but for the case of VV-Pol, similar conclusions can be obtained.

The Doppler frequencies and the spectra bandwidths are further examined in Figs. 9 and 10. The Doppler frequencies and the spectra bandwidths are defined by Eqs. (18) and (19), respectively. Here, the wind speed and the radar frequency are the same as in Fig. 8. From Fig. 9, one can see that for linear surfaces, the Doppler frequencies corresponding to different polarisations first become separated, from each other when the HH-Pol Doppler frequency is getting larger, but eventually come together at low grazing angle, with value close to the Bragg frequency. For

Gerstners sea surfaces, the Doppler frequencies keep growing near low grazing angle. Comparing the results to those obtained by linear surface, we can also find that the results for Gerstners sea surfaces are somewhat larger than their counterparts for linear surface. As shown in Fig. 10, it is obvious that for linear surfaces, the spectra bandwidths increase first to a maximum value and then decrease with increasing the incident angles. However, for Gerstners sea surfaces, it is shown that as the incident angle increases, the spectra bandwidths increase first and then becomes almost a constant. Comparing the simulated results with those obtained by Romeiser–Thompson model,[20] the agreement for Gerstners sea surfaces seems to be better.

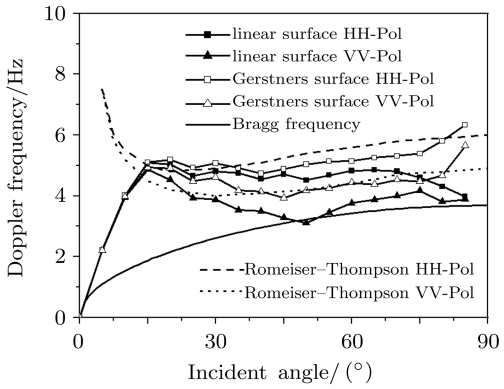


Fig. 9. Doppler frequencies versus incident angle for Gerstners and linear sea surfaces.

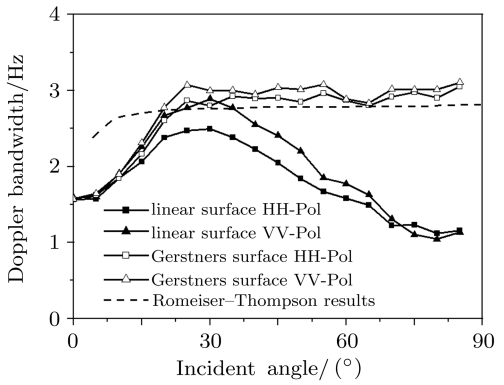


Fig. 10. Spectra bandwidths versus incident angle for Gerstners and linear sea surfaces.

For Gerstners sea surfaces, the issue of spectra bandwidth is further examined in Fig. 11. Here, the incident angle is equal to 85°. It is clear that the spectra bandwidths are getting wider with the increase of the radar frequency. And, we can also find that the spectra bandwidths increase as increasing wind speeds.

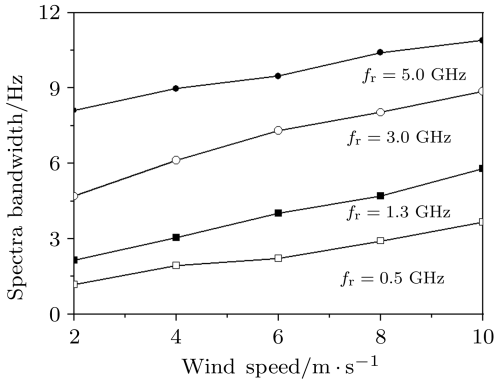


Fig. 11. Spectra bandwidth versus wind speed for different radar frequencies.

5. Conclusions

The scattered fields predicted by SSA-II were in good agreement with the results of direct numerical calculations based on the exact numerical solution of MoM. And the conclusion is obtained that the backscattered NRCSs of Gerstners sea surfaces were somewhat larger than the results from linear sea surfaces as the incident angle is large. We then proceeded with Monte Carlo simulations of average Doppler spectra of backscattered echoes from a time-varying ocean-like surface. The comparisons of Doppler spectra were made for the incidence angles varying from nadir to low grazing and involved linear and Gerstners time-varying sea surfaces. The following conclusions had been obtained: (i) for HF wave, the higher order Doppler peaks for Gerstners sea surfaces were larger than those obtained by linear surfaces due to the nonlinear wave–wave interactions; (ii) for microwave scattered fields, the spectra for Gerstners sea surfaces are considerably broader than their counterparts for the linear surfaces at the large incident angles due to the horizontal components of the small elementary scatterers orbit velocity and the wave–wave interactions in Gerstners sea surface model; (iii) for microwave scattered fields, the spectra will be wider than their counterparts at lower wind speed. Although our studies have been limited to 1-D surfaces, the analysis presented in this work helps to establish a better understanding of the behaviours of scattered fields from an ocean-like surface. In the future, further work should be carried out to investigate the properties of EM scattering by 2-D time-varying Gerstners sea surfaces.

References

[1] Toporkov J V and Brown G S 2000 *IEEE Trans. Geosci. Remote Sensing* **38** 1616

[2] Apel J R 1994 *J. Geophys. Res.* **99** 16269

[3] Rino C L, Crystal T L, Koide A K, Ngo H D and Guthart H 1991 *Radio Sci.* **26** 51

[4] Johnson J T, Toporkov J V and Brown G S 2001 *IEEE Trans. Geosci. Remote Sensing* **39** 2411

[5] Guo L X, Wang R, Wang Y H and Wu Z S 2008 *Acta Phys. Sin.* **57** 3464 (in Chinese)

[6] Guo L X, Wang R, Wang Y H and Wu Z S 2005 *Acta Phys. Sin.* **54** 96 (in Chinese)

[7] Barrick D E 1977 *Remote Sensing Environ.* **6** 201

[8] Barrick D E 1977 *Radio Sci.* **12** 415

[9] Lipa B 1978 *J. Geophys. Res.* **83** 959

[10] Gerstner F J 1809 *Also Reprinted in Ann. der Physik* **32** 412

[11] Rankine W J 1863 *Phil. Trans. R. Soc.* A **153** 127

[12] Voronovich A G and Zavorotny V U 2001 *Waves in Random Media* **11** 247

[13] Wen S C 1962 *Theory of Ocean Waves* (Ji'nan: Shandong Peoples Publishing House) (in Chinese)

[14] Toporkov J V, Awadallah R S and Brown G S 1999 *J. Opt. Soc. Am.* A **16** 176

[15] Longuet-Higgins M S 1975 *J. Geophys. Res.* **80** 2688

[16] Keller M S, Plant W J, Petitt R A and Terray E A 1994 *J. Geophys. Res.* **99** 9751

[17] Bass F G, Fuks I M, Kalmykov A I, Ostrovsky I E and Rosenberg A D 1968 *IEEE Trans. Antennas Propagat.* **16** 554

[18] Derr V E 1972 *Remote Sensing of the Troposphere* (Washington, D.C: U.S.Govt. Printing Office) Chap.12

[19] Lee P H Y, Barter J D, Beach K L, Lake B M, Rungaldier H, Thompson H R, Wang L and Yee R 1999 *Radio Sci.* **34** 123

[20] Romeiser R and Thompson D R 2000 *IEEE Trans. Geosci. Remote Sensing* **38** 446